Journal of Hazardous Materials 168 (2009) 226–232

Contents lists available at ScienceDirect

Journal of Hazardous Materials

journal homepage: www.elsevier.com/locate/jhazmat

# Toluene oxidation on titanium- and iron-modified MCM-41 materials

M. Popova[a,*], Á. Szegedi[b], Z. Cherkezova-Zheleva[c], I. Mitov[c], N. Kostova[c], T. Tsoncheva[a]

[a] Institute of Organic Chemistry with Centre of Phytochemistry, Bulgarian Academy of Sciences, 1113 Sofia, Bulgaria
[b] Institute of Nanochemistry and Catalysis, Chemical Research Center, Hungarian Academy of Sciences, 1025 Budapest, Hungary
[c] Institute of Catalysis, Bulgarian Academy of Sciences, 1113 Sofia, Bulgaria

ARTICLE INFO

*Article history:*
Received 19 November 2008
Received in revised form 26 January 2009
Accepted 3 February 2009
Available online 13 February 2009

*Keywords:*
Total toluene oxidation
Titanium- and iron-modified MCM-41

ABSTRACT

Iron- and titanium-modified MCM-41 materials, prepared by direct synthesis at ambient temperature or wet impregnation technique, were investigated using X-ray diffraction (XRD), transmission electron microscopy (TEM), temperature-programmed reduction (TPR), UV–vis diffuse reflectance, Mössbauer and FT-IR spectroscopies. Their catalytic behavior was studied in total oxidation of toluene. Materials with high surface area and well-ordered pore structure were obtained. The increase of the titanium content (up to 50%) in the bisubstituted, iron and titanium containing materials leads to partial structure collapse of the silica matrix. Finely dispersed anatase particles were also formed during the impregnation procedure. The catalytic activity of the bisubstituted materials was influenced by the method of their preparation, but higher catalytic stability could be achieved, compared to iron monosubstituted one. The nature of the catalytic active sites is discussed.



## 1. Introduction

Volatile organic compounds (VOCs) are the main class of air pollutants, emitted from various industrial processes [1–8]. They include over 300 compounds, such as oxygenates, aromatic and halogen hydrocarbons. The strict regulations on the environmental standards in several countries require a 40% reduction in VOCs emission by 2010. The catalytic total oxidation has been considered as the most appropriate method for VOCs removal and many efforts have been made to design catalysts with good activity and selectivity [1–8]. The commercial catalysts for oxidation of VOC can be classified into three categories: (1) supported noble metals [3,9,10]; (2) metal oxides or supported metals [1,2,4,6,8,11,12]; (3) mixtures of noble metals and metal oxides [13,14]. The noble metals used in practice are Pt and Pd usually supported on oxides ($Al_2O_3$ or $SiO_2$), zeolites (BEA and FAU) [3,9,10]. These catalysts generally show higher activity and selectivity toward total oxidation. Transition metal oxides are one alternative to the noble metal-containing catalysts due to their resistance to halogens, low cost and high catalytic activity and selectivity [2,4,6,8]. Transition metal oxides have been found to be very active, both in total and selective oxidation of hydrocarbons and their catalytic properties can be related to the kind of oxide species involved in the oxidation process [2,4,6]. The nature of the support is also important factor as the surface area and functionality determine the nature and dispersion of the metal oxide particles and therefore their catalytic behavior [1,8]. MCM-41 silica materials, with their uniform mesoporous channel structure and high specific surface area, are of particular interest, as catalyst support [15–22]. A wide variety of metal ions (Fe, Ti, V, Cr, Cu, etc.) has been introduced into the silica matrix to obtain modified mesoporous materials with tunable catalytic properties [23–25]. It has been established, that the applied method of modification strongly influences the state (localization, dispersion and oxidative state) of the loaded metal species [26–29]. Their introduction in the host matrix could be realized during the silica synthesis procedure as well as by various postsynthesis techniques (impregnation and grafting) [26–30]. However, the preparation of stable, modified materials by conventional hydrothermal synthesis is usually possible at low metal loading, which strongly restricts the application as catalysts. It has been reported that the sol–gel technique reveals much higher ability in this aspect and the preparation of stable monocomponent titanium [31]- or iron [26,27]-modified MCM-41 materials has been achieved. Recently, high catalytic activity of mixed iron and titanium oxide bulk materials in oxidative decomposition of chlorobenzene has been reported [32]. Catalytic oxidation of aromatics are in main importance because they are emitted from diverse sources, e.g. from printing, pressing, petrochemical industries, automobile exhaust and traffic-related processes. Total oxidation of toluene has been studied using different metals (Pt, Cu, Fe, V, Co and Cr) on different types of supports ($Al_2O_3$, $CeO_2$ and $TiO_2$ activated carbon) [3,6,8,24]. The Fe-containing catalysts are active in toluene oxidation but the main

* Corresponding author at: Institute of Organic Chemistry with Centre of Phytochemistry, Acad. G. Bonchev str., bl.9, 1113 Sofia, Bulgaria. Tel.: +359 2 979 39 61; fax: +359 2 870 02 25.
*E-mail address:* mpopova@orgchm.bas.bg (M. Popova).

0304-3894/$ – see front matter © 2009 Elsevier B.V. All rights reserved.
doi:10.1016/j.jhazmat.2009.02.018

problem remains the stabilization of the iron species during the catalytic process [8]. To the best of our knowledge no data are available for the catalytic properties of iron- and titanium-modified mesoporous silicas. That is why in this study we focus our attention on the catalytic behavior of iron and titanium substituted mesoporous MCM-41 for oxidative VOCs elimination. Two techniques of samples preparation (conventional impregnation and sol–gel synthesis) were applied. Toluene, which is the main air pollutant was tested as a probe VOC molecule.

## 2. Experimental

### 2.1. Synthesis

The silica MCM-41, the monosubstituted TiMCM-41 and FeMCM-41 materials and the bisubstituted titanium- and iron-containing sample (TiFeMCM-41) were prepared at room temperature by the procedure described in our previous papers [27,33]. Tetraethyl orthosilicate (TEOS, Aldrich) and tetraethyl orthotitanate ($Ti(OEt)_4$, Aldrich) were used as silica and titania source, respectively. Typically, 5.2 ml of TEOS was mixed with 10.4 ml propan-2-ol, 1 ml of $Ti(OEt)_4$ and 0.9 g of $Fe(NO_3)_3{\cdot}9H_2O$. The clear solution was cooled down to 283 K and poured directly to the solution containing 2.5 g N-hexadecyltrimethylammoniumbromide ($C_{16}$TMABr) and 10 ml of conc. ammonia solution (25 wt.%) in 125 ml water. The precipitated suspensions were stirred for 2 h and aged overnight at room temperature. Because of its ammonia content the pH of the synthesis mixture was highly alkaline (about 12) and the synthesis products were washed with distilled water until neutral pH was reached. After drying at 333 K, the template removal was carried out at 813 K in air with a heating rate of 1 K/min. For comparison a sample with higher amount of Ti (Si/Ti = 2) was synthesized by the same procedure. It was denoted as Ti(2)FeMCM-41. Titania impregnated FeMCM-41 sample (Ti/FeMCM41) was prepared by dispersing 1.5 g of FeMCM-41 in 100 ml propan-2-ol and adding 1.3 g of titanium isopropoxide to achieve 25 wt.% $TiO_2$ loading. The slurry was dried while stirring at ambient temperature, than dried at 373 K for 1 h. $TiO_2$ formation was achieved by a heat treatment at 725 K in air for 3 h (2 K/min).

### 2.2. Characterization

X-ray diffractograms were recorded by Philips PW 1810/1870 diffractometer applying monochromatized Cu Kα radiation (40 kV, 35 mA).

TEM images were taken by using a MORGAGNI 268D TEM (100 kV; W filament; point-resolution = 0.5 nm).

Nitrogen physisorption measurements were carried out at 77 K using Quantachrome NOVA Automated Gas Sorption Instrument. The pore-size distributions were calculated from the desorption isotherms with the BJH method.

Chemical composition of the samples were determined by atomic absorption spectroscopy (AAS).

Diffuse reflectance spectra of the samples in the UV–vis region were registered using a Jasco V-570 UV–vis spectrophotometer equipped with NV-470 type integrating sphere. A $BaSO_4$ disk was used as reference. All spectra were recorded under ambient conditions.

The reducibility of the modified samples was investigated by temperature programmed reduction (TPR) technique in $H_2$/Ar flow (10:90, 20 ml/min) using a conventional TPR apparatus equipped with a heat conductivity cell and a trap for removal of released water. The reducibility of the metal oxide species was estimated by measuring the hydrogen uptake of the samples.

The Mössbauer spectroscopic measurements (MS) were made on Wissenschaftliche Elektronic GmbH instrument, operating in a constant acceleration mode ($^{57}$Co/Cr source, α-Fe standard). The following parameters of hyperfine interactions of spectral components were determined by computer fitting: isomer shift (IS), quadrupole splitting (QS), line widths (FW) and component relative weights (G).

FT-IR spectrum was recorded from KBr pellets (99 wt.% of KBr) on a Brucker Vector 22.

### 2.3. Catalytic activity measurements

Prior to the catalytic test the samples were pretreated for 1 h in air up to 723 K. Toluene oxidation was studied at atmospheric pressure using a fixed-bed flow reactor, air as carrier gas and 30 mg sample (particle size 0.2–0.8 mm) diluted with 60 mg glass beads of the same diameter previously checked to be inactive. The air stream passed through a saturator filled with toluene and equilibrated at 273 K ($p_{toluene}$ = 0.9 kPa). The activity was determined in the temperature interval of 623–723 K at WHSV of 1.2 $h^{-1}$. On-line analysis of the reaction products was performed using HP-GC with a 25 m PLOT Q capillary column. The turnover frequency (TOF) was calculated as the converted number of toluene molecules per an iron atom per a second. Only in the case of monocomponent Ti material the calculations were done per Ti atom. In some runs, after removing the catalyst from the reactor, the coke was analyzed by thermogravimetry using a SETARAM TG-DTG 92 thermobalance. Coked samples were heated from room temperature to 873 K under air flow with a temperature increase of 10 K/min.

## 3. Results and discussion

### 3.1. Physico-chemical characterization of the samples

Small angle XRD patterns (Fig. 1) of parent silica material exhibit reflections typical of hexagonally arranged pore structure, which is almost preserved after the modification. The shift of the position of the (1 0 0) reflection for the modified materials in comparison with the parent one could be assigned to the incorporation of the metal ions in the silica framework. Higher degree of titanium incorporation could be concluded in the case of bisubstituted directly synthesized material, where more distinguished shift of the SAXS reflection to smaller 2$\theta$, in comparison with pure MCM-41 (Fig. 1) is observed. Partial silica matrix collapse can be assumed only for Ti(2)FeMCM-41, where the disappearance of the (1 0 0) reflection confirms the long range ordering decrease of the structure. In the wide-angles region no characteristic reflections of any iron and/or titanium containing species are registered, which suggests their predominant incorporation into the MCM-41 silica framework. Only in the case of Ti/FeMCM-41 wide reflections of anatase phase are observed.

TEM images of the modified MCM-41 silica materials (Fig. 2) confirm the preservation of the support mesoporous structure. In accordance with XRD data (Fig. 1) the dark spots in the TEM image, which are distinguished for Ti/FeMCM-41 could be assigned to the presence of anatase particles, probably below 10 nm.

In Fig. 3, nitrogen physisorption isotherms and pore size distribution of the parent and modified silica materials are presented. The corresponding calculated parameters are listed in Table 1. The isotherm of parent MCM-41 silica is of type IV (IUPAC classification), with a sharp capillary condensation step at about 0.25 $p/p_0$, characteristic of mesoporous materials with narrow pore size distribution. After the modification, the isotherms preserve their shape, indicating the mesoporous structure preservation. Only in the case of the sample with the highest titanium content, Ti(2)FeMCM-41,

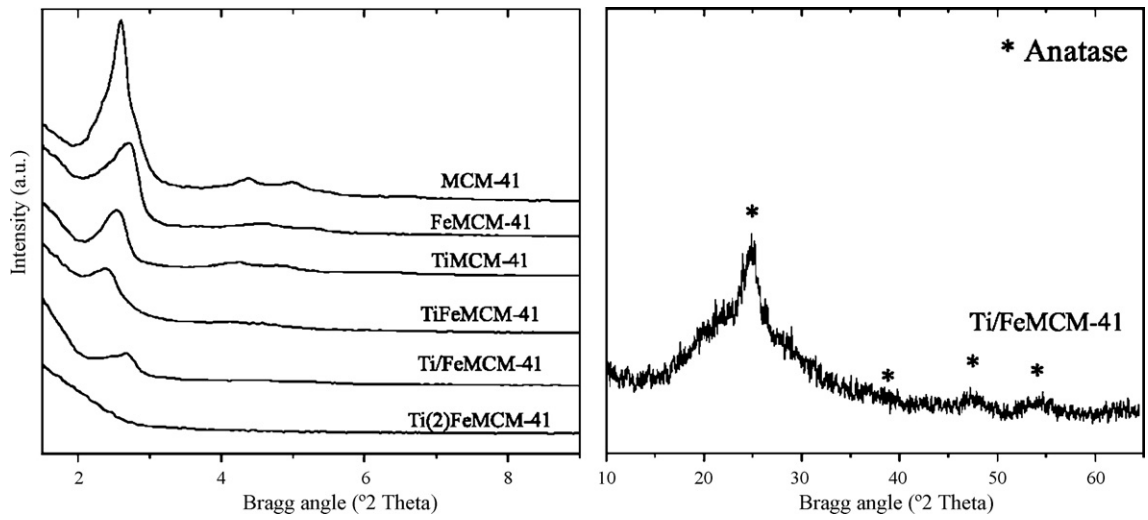


**Fig. 1.** XRD patterns of the studied samples.

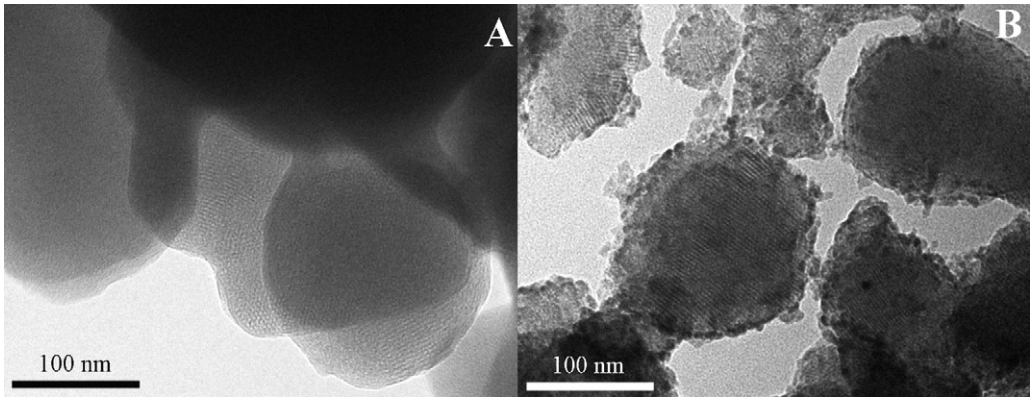


**Fig. 2.** TEM images of the sol–gel prepared (A) and the impregnated (B) bisubstituted samples.

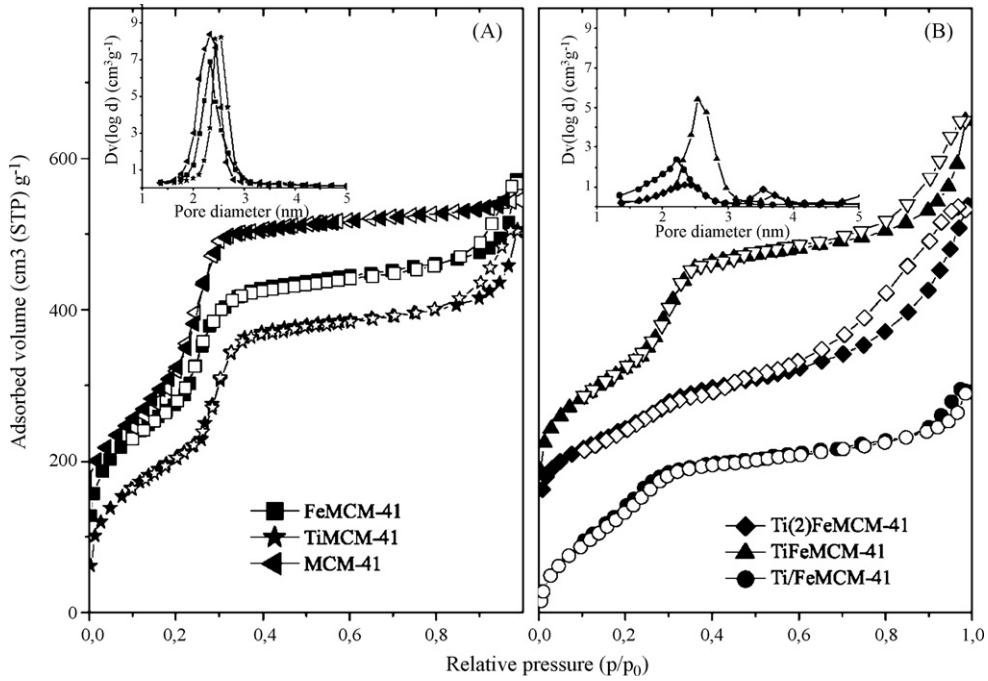


**Fig. 3.** Nitrogen adsorption/desorption isotherms (the curves are shifted in *y*-direction in order to prevent overlapping) of the initial, monosubstituted (A) and bisubstituted (B) materials.

**Table 1**
Physico-chemical properties of the studied samples.

| Samples | Si/Fe | Si/Ti | Fe cont.[a] (mmol/$g_{calc}$) | $S_{BET}$ ($m^2$/g) | PD[b] (nm) | Pore vol.[b] ($cm^3$/g) | $a_0$[c] (nm) |
|---|---|---|---|---|---|---|---|
| SiMCM-41 | – | – | – | 1198 | 2.3 | 1.0 | 3.94 |
| FeMCM-41 | 20 | – | 0.78 | 984 | 2.3 | 0.92 | 3.95 |
| Ti/FeMCM-41 | 20 | 4 | 0.62 | 880 | 2.2 | 0.62 | 3.83 |
| TiFeMCM-41 | 20 | 10 | 0.68 | 852 | 2.5 | 0.91 | 3.95 |
| Ti(2)FeMCM-41 | 20 | 2 | 0.48 | 573 | 2.3 | 0.71 | – |
| TiMCM-41 | – | 10 | – | 907 | 2.6 | 0.90 | 4.06 |

[a] Related to 1 g calcined at 1273 K.
[b] Pore diameter and pore volume calculated by BJH method (desorption branch).
[c] Cell parameter ($a_0 = 2d_{100}(3)^{-1/2}$).

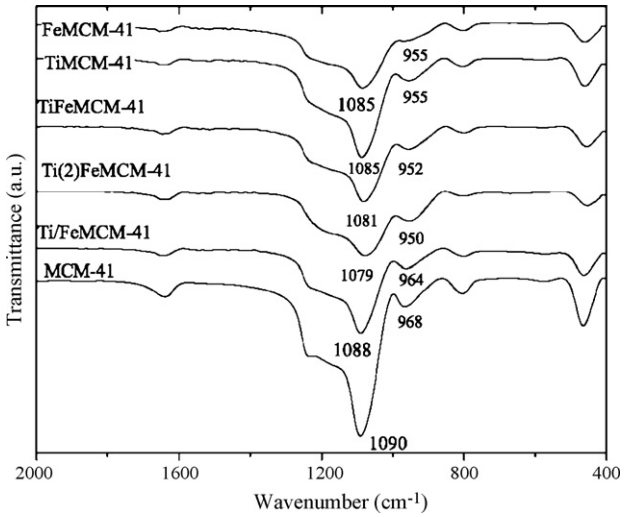


**Fig. 4.** FT-IR spectra of the initial and modified samples.

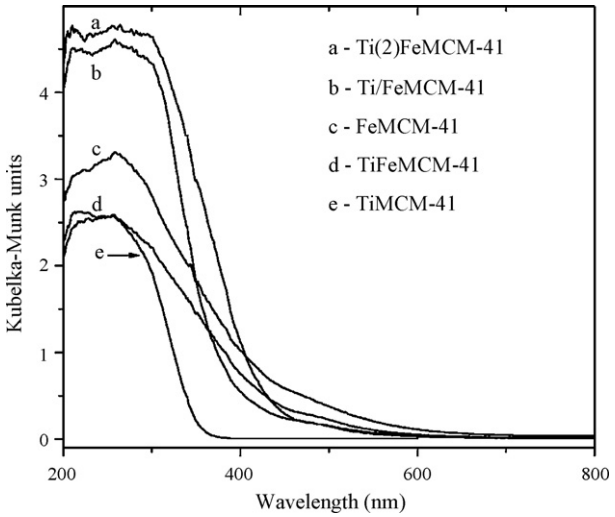


**Fig. 5.** UV–vis spectra of the mono- and bisubstituted materials.

a partial structure collapse (Table 1) could be assumed, which is in accordance with the XRD measurements. The impregnated sample, Ti/FeMCM-41, exhibits a simultaneous decrease in the pore volume and average pore diameter, indicating a partial pore blocking due to the deposition of anatase particles.

In Fig. 4, the FT-IR spectra of parent and modified materials are compared. The asymmetric stretching vibrations of Si–O–Si from the silica matrix appear at about 1090 $cm^{-1}$. The slight shift of this band to lower wavenumbers is observed for the sol–gel synthesized materials. The band at 968 $cm^{-1}$ probably arises from both Si–O–H and Si–O–M stretching vibrations. The simultaneous shift of the band at 1090 $cm^{-1}$ and the band at 968 $cm^{-1}$ to the lower wavenumbers is usually ascribed to the presence of tetrahedrally coordinated metal ions in the silica matrix [21]. The negligible changes in the spectrum of Ti/FeMCM-41 in comparison with the initial MCM-41 silica confirm the lower degree of titanium incorporation into the silica matrix.

The UV–vis spectra (Fig. 5) of both monosubstituted materials exhibit a broad absorption peak in the 210–250 nm region attributable to isolated, tetrahedrally coordinated metal species [20,21,31,34]. According to [20,34], the bands at about 350 nm, which are detected for all iron-modified materials, most probably arise from the presence of oligomeric $FeO_x$ species and finely dispersed hematite like nanoparticles, respectively. The intensive absorption band at about 330 nm for Ti/FeMCM-41 indicates the formation of anatase particles and confirms the results obtained by XRD and TEM measurements (see above).

Mössbauer spectroscopy is applied for more detailed characterization of the iron species. The spectra of all studied materials consist only of doublet-lines. Their optimal mathematical treatment represents two doublet components with different relative weight. The determined hyperfine parameters of the two sets of doublets (Table 2) show the presence of high spin $Fe^{3+}$ ions in tetrahedral (Dbl 1) and octahedral (Dbl 2) oxygen coordination, respectively. According to [19,35–37], Dbl 1 can be assigned to iron species isomorphously incorporated into the silica framework. The interpretation of Dbl 2 is more complicated. On one hand, its parameters could be indicative for the presence of finely dispersed iron oxide nanoparticles ($D < 10$ nm) with superparamagnetic behavior. On the other hand, according to [37], Dbl 2 could also be assigned to $Fe^{3+}$ ions incorporated in the silica framework, completing their coordination spheres to octahedral with adsorbed water molecules.

In Fig. 6, the TPR profiles of the modified materials are presented. All iron containing samples show a well pronounced TPR peak

**Table 2**
Redox properties of titanium- and iron-modified MCM-41 materials.

| Samples | $H_2$ uptake[a] (mmol/$g_{calc}$) | Extent of reduction[b] (%) | C[c] (wt.%) |
|---|---|---|---|
| SiMCM-41 | – | – | – |
| FeMCM-41 | 0.42 | 100 | 1.11 |
| Ti/FeMCM-41 | 0.31 | 100 | 0 |
| TiFeMCM-41 | 0.21 | 62.0 | 6.60 |
| Ti(2)FeMCM-41 | 0.19 | 79.7 | 8.83 |
| TiMCM-41 | 0.05 | 7.9 | 4.65 |

[a] Calculated from the area of the TPR curve in the range of 373–1073 K.
[b] Calculated from the $H_2$ uptake related to the total amount of iron (see Table 1) and titanium (1.39 mmol/g), assuming that 1 mmol $H_2$ is needed for the reduction of 2 mmol $Fe^{3+}$ to $Fe^{2+}$ and 2 mmol $Ti^{4+}$ to $Ti^{3+}$ for the Fe-containing samples and TiMCM-41, respectively.
[c] Amount of coke formed during the 240 min reaction at 613 K.

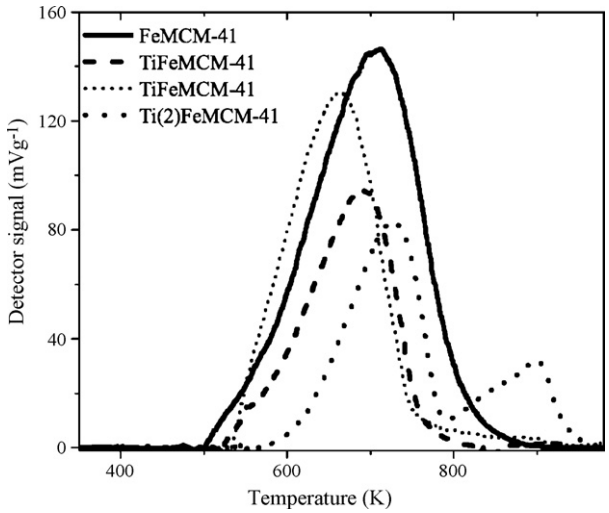


**Fig. 6.** TPR profiles of various modified samples.

between 500 and 870 K. The calculated hydrogen uptake (Table 2) for FeMCM-41 corresponds to one electron transfer, i.e. $Fe^{3+}$ ions could be reduced only to $Fe^{2+}$ state up to 870 K [35,37]. The lower hydrogen uptake, which is registered for bisubstituted directly synthesised materials in comparison with FeMCM-41, could be assigned to the more difficult reduction of the iron species in the case of the former materials (Fig. 6, Table 2). Changes of the iron environment, probably due to the formation of –Ti–O–Fe– type species, can be responsible for this decreased reducibility. The hydrogen uptake at lower temperature and higher degree of reduction (about 100%) that is found for Ti/FeMCM-41 (Fig. 6B) could be assigned to the presence of easily reducible iron oxide species in it. This effect confirms the limited formation of –Ti–O–Fe– type species during the impregnation technique. The calculated extent of reduction for TiMCM-41 is significantly lower in comparison to all iron-containing samples (Table 2).

### 3.2. Catalytic activity for toluene oxidation

In Fig. 7A, the temperature dependencies of toluene oxidation on various modified MCM-41 materials are presented. $CO_2$ is the only registered product in all cases. For the monosubstituted samples, the titanium containing one exhibits lower catalytic activity and it remains almost unchanged with time on stream (Fig. 7B). In contrast, a well-defined trend to catalytic activity decrease is registered for FeMCM-41 (Fig. 7B). Among the modified materials, Ti/FeMCM-41 possesses the best catalytic activity and stability. Lower catalytic activity but higher stability in comparison with FeMCM-41 is observed for bisubstituted materials, prepared by direct synthesis. A well-pronounced increase in the catalytic activity with time on stream is registered for these samples as well. The catalytic activity significantly decreases with the increase of the titanium content, which could be due to the lower BET surface area and the high degree of structure collapse in this case (see XRD, $N_2$ physisorption data). The hydrogen pretreatment at 723 K leads to an increase in the catalytic activity of TiMCM-41 and to its decrease for the iron containing materials (Fig. 7B). Only in the case of Ti/FeMCM-41 a negligible effect of preliminary reduction is observed.

After the catalytic tests some structural changes of the samples could be observed. The Mössbauer spectra (Table 3) exhibited increasing relative part of the octahedrally coordinated iron ions, which could be ascribed to their partial release from framework positions. These changes are negligible for TiFeMCM-41 that confirms the favorable effect of titanium incorporation for the stabilization of iron ions in framework positions. The appearance of a new doublet component with a higher isomer shift, that is registered only for the sample with a partial structure collapse, Ti(2)FeMCM-41, could be ascribed to $Fe^{2+}$ ions. The DTG analysis in air of the materials used in catalytic tests, point to the presence of non-desorbed products, which can be found in higher amount on the samples possessing lower catalytic activity (Table 2). Formation of coke precursors, probably due to the oligomerization of intermediate products of the total toluene oxidation is expected [35,38]. This coke deposition could be considered as a reason for the reduction transformations of the samples during the catalytic tests (Table 3).

Summarizing the catalytic performance and physicochemical analysis of the modified materials, the simultaneous participation of different catalytically active sites could be assumed. The activity of $Fe^{3+}$–$Fe^{2+}$ and $Ti^{3+}$–$Ti^{4+}$ redox ion couples is expected in the case of FeMCM-41 and TiMCM-41, respectively. According to Mars-van-Krevelen mechanism, which is usually realized during the toluene oxidation [39–42], the participation of oxygen from the solid cata-

**Table 3**
Mössbauer parameters for the modified MCM-41 materials.

| Sample | Components | IS (mm/s) | QS (mm/s) | FWHM (mm/s) | G (%) |
|---|---|---|---|---|---|
| TiFeMCM-41 | Db 1–$Fe^{3+}$ tetra | 0.27 | 1.01 | 0.58 | 35 |
| | Db 2–$Fe^{3+}$ octa | 0.38 | 1.04 | 0.52 | 65 |
| TiFeMCM-41, after catalytic experiment | Db 1–$Fe^{3+}$ tetra | 0.22 | 1.02 | 0.48 | 34 |
| | Db 2–$Fe^{3+}$ octa | 0.39 | 1.03 | 0.51 | 66 |
| Ti(2)FeMCM-41 | Db 1–$Fe^{3+}$ tetra | 0.29 | 1.01 | 0.64 | 36 |
| | Db 2–$Fe^{3+}$ octa | 0.38 | 1.11 | 0.58 | 64 |
| Ti(2)FeMCM-41, after catalytic experiment | Db 1–$Fe^{3+}$ tetra | 0.29 | 0.97 | 0.61 | 34 |
| | Db 2–$Fe^{3+}$ octa | 0.35 | 1.20 | 0.62 | 54 |
| | Db 3–$Fe^{2+}$ | 1.07 | 2.17 | 0.35 | 11 |
| FeMCM-41 | Db 1–$Fe^{3+}$ tetra | 0.22 | 1.08 | 0.47 | 33 |
| | Db 2–$Fe^{3+}$ octa | 0.38 | 1.02 | 0.50 | 67 |
| FeMCM-41, after catalytic experiment | Db 1–$Fe^{3+}$ tetra | 0.22 | 1.14 | 0.56 | 26 |
| | Db 2–$Fe^{3+}$ octa | 0.38 | 1.15 | 0.59 | 74 |
| Ti/FeMCM-41 | Db 1–$Fe^{3+}$ tetra | 0.28 | 0.81 | 0.50 | 33 |
| | Db 2–$Fe^{3+}$ octa | 0.38 | 1.01 | 0.59 | 67 |
| Ti/FeMCM-41, after catalytic experiment | Db 1–$Fe^{3+}$ tetra | 0.27 | 1.05 | 0.55 | 30 |
| | Db 2–$Fe^{3+}$ octa | 0.38 | 1.09 | 0.63 | 70 |

Isomer shift related to iron (IS); quadropole splitting (QS); full line width at half maximum (WHM); relative weight of the partial components in the spectra (G).

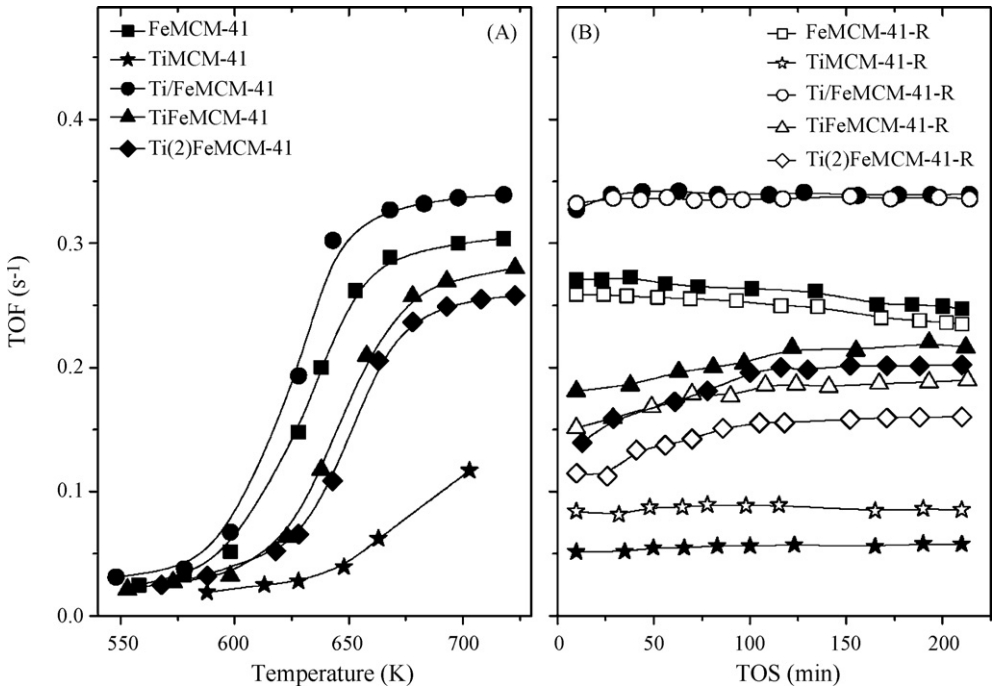


**Fig. 7.** Catalytic activity *vs.* temperature (A) and time on stream at 673 K (B) on the modified materials before and after pretreatment in hydrogen at 723 K.

lyst is of key importance. In this aspect, the higher catalytic activity of FeMCM-41 could be assigned to the easier release of oxygen from the modified silica lattice, probably due to the higher polarization of the Fe–O–Si bond in comparison to the Ti–O–Si one. This assumption is supported by the easier reducibility of the iron-modified MCM-41 (see TPR data). The intermediate catalytic activity that was observed for the directly modified bisubstituted materials in comparison with their monosubstituted analogues could be ascribed to the presence of hardly reducible active sites, probably type Fe–O–Ti (see TPR data). The electron transitions types of $Fe^{2+}$–$Ti^{4+}$ and $Fe^{3+}$–$Ti^{3+}$ could be suggested in them during the redox process. These transitions seem to be favored for the hydrogen pretreated materials (Fig. 7B). The facilitated effect of the formed Fe–O–Ti species on the catalytic stability should also be stressed (Fig. 7B). In the case of monosubstituted iron containing material (FeMCM-41) the catalytic activity decrease could be assigned to the partial iron release from the tetrahedral position (Table 3), most probably with the formation of hematite like nanoparticles. Such hematite like nanoparticles seem to be also formed in the impregnated sample, Ti/FeMCM41, and this is confirmed by the decreased relative part of the tetrahedrally coordinated iron species in the Mössbauer spectra after the catalytic test (Table 3). These transformations could be due to the influence of the reaction and pretreatment media or the water formed in the reaction, leading to the formation of hematite-like nanoparticles. Their deposition on the anatase phase could be a reason for the increased catalytic activity. Here, the titania support effect on the hematite like nanoparticles, resulted in facilitated oxygen release from the iron oxide species, could be suggested and it is confirmed by the sample's easier reducibility (see TPR data).

## 4. Conclusion

The method of MCM-41 modification with iron and/or titanium influences the state of the metal species in the silica matrix. Formation of $Fe^{3+}$ and $Ti^{4+}$ ions in tetrahedral position is registered for all materials prepared by direct sol–gel synthesis. Partial structure collapse of the silica matrix is observed with the increase in the titanium content (up to 50%). The introduction of titanium in the iron-modified MCM-41 by impregnation technique leads to additional formation of finely dispersed anatase nanoparticles. The highest catalytic activity is observed for the sample obtained by impregnation procedure. Bisubstituted materials obtained by direct sol–gel synthesis possess lower catalytic activity, but higher stability in total toluene oxidation in comparison with the monosubstituted iron material. Simultaneous participation of iron-, titanium- and mixed iron–titanium active sites is assumed.

## Acknowledgements

Financial support by BY–X–305/07, Hungarian Research Fund, OTKA (grant F 61972), National Office for Research and Technology (NKTH, GVOP project no. 3.2.1. 2004-04-0277/3.0) and the Bulgarian–Hungarian Inter-academic Exchange Agreement are greatly acknowledged.

## References

[1] F. Bertinchamps, C. Gregoire, E.M. Gaineaux, Systematic investigation of supported transition metal oxide based formulations for the catalytic oxidative elimination of (chloro)-aromatics. Part II. Influence of the nature and addition protocol of secondary phases to $VO_x/TiO_2$, Appl. Catal. B 66 (2006) 10–22.
[2] Ch.-H. Wang, Sh.-Sh. Lin, Ch.-L. Chen, H.-Sh. Weng, Performance of the supported copper oxide catalysts for the catalytic incineration of aromatic hydrocarbons, Chemosphere 64 (2006) 503–509.
[3] A.A. dos Santos, K.M. Lima, R.T. Figueiredo, S.M.da.S. Egues, A.L.D. Ramos, Toluene deep oxidation over noble metals, Copper and Vanadium Oxides, Catal. Lett. 114 (2007) 59–63.
[4] R.S.G. Ferreira, P.G.P. de Oliveira, F.B. Noronha, The effect of the nature of vanadium species on benzene total oxidation, Appl. Catal. B 29 (2001) 275–283.
[5] M.A. Centeno, M. Paulis, M. Montes, J.A. Odriozola, Catalytic combustion of volatile organic compounds on $Au/CeO_2/Al_2O_3$ and $Au/Al_2O_3$ catalysts, Appl. Catal. A 234 (2002) 65–78.
[6] V. Gaur, A. Sharma, N. Verma, Catalytic oxidation of toluene and *m*-xylene by activated carbon fiber impregnated with transition metals, Carbon 43 (2005) 3041–3053.
[7] Sh. Yuan, Q. Sheng, J. Zhang, H. Yamashita, D. He, Synthesis of thermally stable mesoporous $TiO_2$ and investigation of its photocatalytic activity, Micropor. Mesopor. Mater. 110 (2008) 501–507.
[8] S.Ch. Kim, W.G. Shim, Influence of physicochemical treatments on iron-based spent catalyst for catalytic oxidation of toluene, J. Hazard. Mater. 154 (2007) 310–316.

[9] M. Zhang, B. Zhou, K.T. Chuang, Catalytic deep oxidation of volatile organic compounds over fluorinated carbon supported platinum catalysts at low temperatures, Appl. Catal. B: Environ. 13 (1997) 123–130.
[10] J.C.-S. Wu, T.-Y. Chang, VOC deep oxidation over Pt catalysts using hydrophobic supports, Catal. Today 44 (1998) 111–118.
[11] K.M. Parida, A. Samal, Catalytic combustion of volatile organic compounds on Indian Ocean manganese nodules, Appl. Catal. A: Gen. 182 (1999) 249–256.
[12] P. Papaefthimiou, T. Ioannides, X.E. Verykios, Combustion of non-halogenated volatile organic compounds over group VIII metal catalysts, Appl. Catal. B: Environ. 13 (1997) 175–184.
[13] M.M.R. Feijen-Jeurissen, J.J. Jorna, B.E. Nieuwenhuys, G. Sinquin, C. Petit, J.-P. Hindermann, Mechanism of catalytic destruction of 1,2-dichloroethane and trichloroethylene over g-Al2O3 and g-Al2O3 supported chromium and palladium catalysts, Catal. Today 54 (1999) 65–79.
[14] S.K. Gangwal, M.E. Mullins, J.J. Spivey, P.R. Caffrey, B.A. Tichenor, Kinetics and selectivity of deep catalytic oxidation of *n*-hexane and benzene, Appl. Catal. 36 (1988) 231.
[15] A. Corma, From microporous to mesoporous molecular sieve materials and their use in catalysis, Chem. Rev. 97 (1997) 2373–2420.
[16] Y. Wang, Q. Zhang, T. Shishido, K. Takehira, Characterizations of iron-containing MCM-41 and its catalytic properties in epoxidation of styrene with hydrogen peroxide, J. Catal. 209 (2002) 186–196.
[17] Ch. Wu, Y. Kong, F. Gao, Y. Wu, Y. Lu, J. Wang, L. Dong, Synthesis, characterization and catalytic performance for phenol hydroxylation of Fe-MCM41 with high iron content, Micropor. Mesopor. Mater. 113 (1–3) (2008) 163–170.
[18] W.A. Garvalho, P.B. Varaldo, M. Wallau, U. Schuchardt, Mesoporous redox molecular sieves analogous to MCM-41, Zeolites 18 (1997) 408–416.
[19] T. Kawabata, Y. Ohishi, S. Itsuki, N. Fujisaki, T. Shishido, K. Takaki, Q. Zhang, Y. Wang, K. Takehira, Iron-containing MCM-41 catalysts for Baeyer–Villiger oxidation of ketones using molecular oxygen and benzaldehyde, J. Mol. Catal. 236 (2005) 99–106.
[20] M.S. Hamdy, G. Mul, J.C. Jansen, A. Ebaid, Z. Shan, A.R. Overweg, Th. Maschmeyer, Synthesis, characterization, and unique catalytic performance of the mesoporous material Fe-TUD-1 in Friedel–Crafts benzylation of benzene, Catal. Today 100 (2005) 255–260.
[21] A. Orlov, Q.-Z. Zhal, J. Klinowski, Photocatalytic properties of the SBA-15 mesoporous silica molecular sieve modified with titanium, J. Mater. Sci. 41 (2006) 2187–2193.
[22] R.S. Araujo, D.C.S. Azevedo, E. Rodrıguez-Castellon, A. Jimenez-Lopez, C.L. Cavalcante Jr., Al and Ti-containing mesoporous molecular sieves: synthesis, characterization and redox activity in the anthracene oxidation, J. Mol. Catal. 281 (2008) 154–163.
[23] A. Taguchi, F. Schüth, Ordered mesoporous materials in catalysis, Micropor. Mesopor. Mater. 77 (2005) 1–45.
[24] A.C.C. Rodriguis, Metallic mixed oxides (Pt, Mn or Cr) as catalysts for the gas-phase toluene oxidation, Catal. Commun. 8 (2007) 1227–1231.
[25] I. Sobczak, M. Ziolek, M. Renn, P. Decyk, I. Nowak, M. Daturi, J.-C. Lavalley, Cu state and behaviour in MCM-41 mesoporous molecular sieves modified with copper during the synthesis––comparison with copper exchanged materials, Micropor. Mesopor. Mater. 74 (2004) 23–36.
[26] A. Szegedi, M. Hegedűs, J.L. Margitfalvi, I. Kiricsi, Low temperature CO oxidation over iron-containing MCM-41 catalysts, Chem. Commun. 11 (2005) 1441–1443.
[27] A. Szegedi, Y. Kónya, D. Méhn, E. Solymár, G. Pal-Borbély, Y. Horváth, L. Biró, I. Kiricsi, Spherical mesoporous MCM-41 materials containing transition metals: synthesis and characterization, Appl. Catal. A 272 (1–2) (2004) 257–266.
[28] M. Kang, M.-H. Lee, Synthesis and characterization of Al-, Bi-, and Fe-incorporated mesoporous titanosilicate (MPTS) materials and their hydrophilic properties, Appl. Catal. A 284 (2005) 215–222.
[29] M. Zhou, J. Yu, B. Chang, Effects of Fe-doping on the photocatalytic activity of mesoporous $TiO_2$ powders prepared by an ultrasonic method, J. Hazard. Mater. B 137 (2006) 1838–1847.
[30] N.B. Lihitkar, M.K. Abyaneh, V. Samuel, R. Pasricha, S.W. Gosavi, S.K. Kulkarni, Titania nanoparticles synthesis in mesoporous molecular sieve MCM-41, J. Colloid Interface Sci. 314 (2007) 310–316.
[31] C. Galacho, M.M.L.R. Carrott, P.J.M. Carrot, Structural and catalytic properties of Ti–MCM-41 synthesised at room temperature up to high Ti content, Micropor. Mesopor. Mater. 100 (1–3) (2007) 312–321.
[32] A. Khaleel, A. Al-Nayli, Supported and mixed oxide catalysts based on iron and titanium for the oxidative decomposition of chlorobenzene, Appl. Catal. 80 (2008) 176–184.
[33] M. Popova, A. Szegedi, N. Kostova, T. Tsoncheva, Titanium modified MCM-41 as a catalyst for toluene oxidation, Catal. Commun. 10 (2008) 304–308.
[34] L. Chmielarz, P. Kustrowski, M. Drozdek, R. Dziembaj, P. Cool, E.F. Vansant, Selective catalytic oxidation of ammonia into nitrogen over PCH modified with copper and iron species, Catal. Today 114 (2006) 319–325.
[35] A. Szegedi, G. Pal-Borbely, K. Lazar, Comparison of the redox properties of iron incorporated in different amounts into MCM-41, React. Kinet. Catal. Lett. 74 (2001) 277–287.
[36] S. Dzwigaj, L. Stievano, F.E. Wagner, M. Che, Effect of the preparation and metal content on the introduction of Fe in BEA zeolite, studied by DR UV–vis, EPR and Möesbauer spectroscopy, J. Phys. Chem. Solids 68 (2007) 1885–1891.
[37] K. Lazar, P. Fejes, G. Pal-Borbely, H.K. Beyer, Hyperfine Interact. 141/142 (2002) 387–390.
[38] A.P. Antunes, M.F. Ribeiro, J.M. Silva, F.R. Ribeiro, P. Magnoux, M. Guisnet, Catalytic oxidation of toluene over CuNaHY zeolites: coke formation and removal, Appl. Catal. B 33 (2001) 149–164.
[39] L.C.A. Oliveira, R.M. Lago, J.D. Fabris, K. Sapag, Catalytic oxidation of aromatic VOCs with Cr or Pd-impregnated Al-pillared bentonite: byproduct formation and deactivation studies, Appl. Clay Sci. 39 (2007) 218–222.
[40] S.H. Taylor, C.S. Heneghan, G.J. Hutchings, I.D. Hudson, The activity and mechanism of uranium oxide catalysts for the oxidative destruction of volatile organic compounds, Catal. Today 59 (2000) 249–259.
[41] S. Minico, S. Scire, C. Crisafulli, R. Maggiore, S. Galvagno, Catalytic combustion of volatile organic compounds on gold/iron oxide catalysts, Appl. Catal. B 28 (2000) 245–251.
[42] E.M. Cordi, P.J. O'Neill, J.L. Falconer, Transient oxidation of volatile organic compounds on a$CuO/Al_2O_3$ catalyst, Appl. Catal. B 14 (1997) 23–36.